Composites: Part A 39 (2008) 1037–1053

Contents lists available at ScienceDirect

Composites: Part A

journal homepage: www.elsevier.com/locate/compositesa

Characterization of mechanical behavior of woven fabrics: Experimental methods and benchmark results

J. Cao [a,*], R. Akkerman [b], P. Boisse [c,1], J. Chen [d], H.S. Cheng [a], E.F. de Graaf [b], J.L. Gorczyca [d], P. Harrison [e], G. Hivet [c], J. Launay [c], W. Lee [a], L. Liu [d], S.V. Lomov [f], A. Long [e], E. de Luycker [c], F. Morestin [c], J. Padvoiskis [a], X.Q. Peng [a], J. Sherwood [d], Tz. Stoilova [f], X.M. Tao [g], I. Verpoest [f], A. Willems [f], J. Wiggers [e], T.X. Yu [g], B. Zhu [g]

[a] Department of Mechanical Engineering, Northwestern University, 2145 Sheridan Road, Evanston, IL 60208, USA[2]
[b] University of Twente, Faculty of Engineering Technology, Drienerlolaan 5, P.O. Box 217, 7500AE, Enschede, Netherlands[3]
[c] LaMCoS, INSA-Lyon, Bâtiment Jacquard, Rue Jean Capelle, F69621 Villeurbanne Cedex, France[4]
[d] Advanced Composite Materials and Textile Research Laboratory, University of Massachusetts Lowell, One University Avenue, Lowell, MA 01854, USA[5]
[e] School of Mechanical, Materials and Manufacturing Engineering, University of Nottingham, University Park, Nottingham NG7 2RD, UK[6]
[f] Katholieke Universiteit Leuven, Department of Metallurgy and Materials Engineering, Kasteelpark Arenberg 43, BE-3001 Heverlee, Belgium[7]
[g] Department of Mechanical Engineering, Hong Kong University of Science and Technology, Clear Water Bay, Kowloon, Hong Kong[8]

ARTICLE INFO

Article history:
Received 27 September 2007
Received in revised form 26 February 2008
Accepted 26 February 2008

Keywords:
A. Fabrics/textile
B. Mechanical properties
D. Mechanical testing
E. Forming

ABSTRACT

Textile composites made of woven fabrics have demonstrated excellent mechanical properties for the production of high specific-strength products. Research efforts in the woven fabric sheet forming are currently at a point where benchmarking will lead to major advances in understanding both the strengths and the limitations of existing experimental and modeling approaches. Test results can provide valuable information for the material characterization and forming process design of woven composites if researchers know how to interpret the results obtained from varying test methods appropriately. An international group of academic and industry researchers has gathered to design and conduct benchmarking tests of interest to the composite sheet forming community. Shear deformation is the dominative deformation mode for woven fabrics in forming; therefore, trellis-frame (picture-frame) and bias-extension tests for both balanced and unbalanced fabrics have been conducted and compared through this collaborative effort. Tests were conducted by seven international research institutions on three identical woven fabrics. Both the variations in the setup of each research laboratory and the normalization methods used to compare the test results are presented and discussed. With an understanding of the effects of testing variations on the results and the normalization methods, numerical modeling efforts can commence and new testing methods can be developed to advance the field.

1. Introduction

Woven-fabric reinforced composites (hereafter referred to as textile composites) have attracted a significant amount of attention from both industry and academia due to their high specific strength and stiffness, as well as their supreme formability characteristics. Woven fabrics (Fig. 1) are created by weaving yarn into a repeating pattern. Yarn is made of continuous or stretchable fibers with diameters typically in the order of micron meters (μm). The manufacture of components from woven fabrics involves a forming stage in which the fabric is deformed into a desired shape either (a) by a punch with the fabric being subjected to a binder holding force as illustrated in Fig. 2 or (b) by machine or manual laying-up where the fabric can be subjected to either complex edge stretching or no stretching. This step can be performed at room temperature for dry fabric or at elevated temperatures (i.e., thermoforming) for fabrics made of glass/carbon fibers commingled with thermoplastic fibers. The formed fabric can further be injected with resin and consolidated in a resin transfer molding (RTM) process, a liquid composite molding (LCM) process [1,2].

Commercial applications for textile composites include products for energy absorption (e.g., helmet) [4], aerospace and defense

* Corresponding author. Tel.: +1 847 467 1032; fax: +1 847 491 3915.
E-mail addresses: jcao@northwestern.edu (J. Cao), r.akkerman@ctw.utwente.nl (R. Akkerman), philippe.boisse@insa-lyon.fr (P. Boisse), julie_chen@uml.edu (J. Chen), stepan.lomov@mtm.kuleuven.ac.be (S.V. Lomov), andrew.long@nottingham.ac.uk (A. Long), metxyu@ust.hk (T.X. Yu).

[1] Formerly at aboratoire de Mécanique des Systèmes et des Procédés, Paris, France.
[2] http://www.mech.northwestern.edu/fac/cao/.
[3] http://www.opm.ctw.utwente.nl/en/pt/.
[4] http://www.lamcos.insa-lyon.fr/.
[5] http://www.m-5.eng.uml.edu/acmtrl/.
[6] http://www.textiles.nottingham.ac.uk/.
[7] http://www.mtm.kuleuven.ac.be/research/c2/poly.
[8] http://www.me.ust.hk/.

1359-835X/$ - see front matter © 2008 Elsevier Ltd. All rights reserved.
doi:10.1016/j.compositesa.2008.02.016

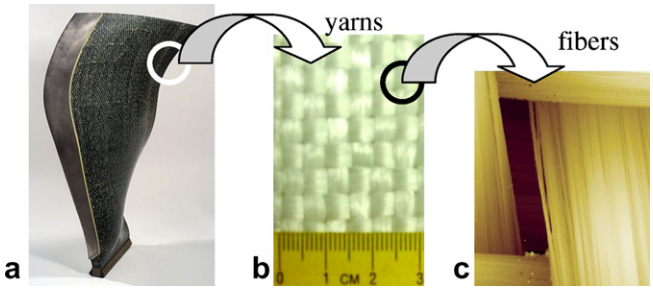

Fig. 1. (a) A textile composites fan made by SNECMA, (b) woven fabric and (c) fibers in woven fabric.

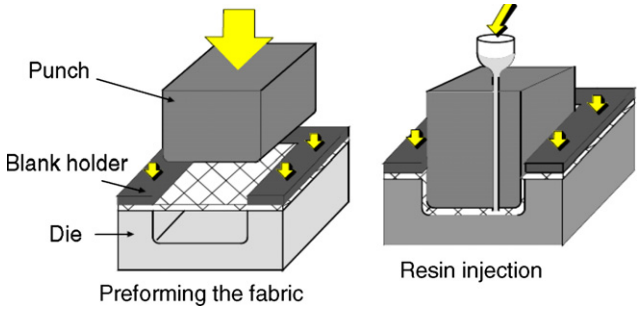

Fig. 2. Schematics of performing and resin injection molding processes [3].

applications (e.g., engine inlet cowlings, fuselage sections, rotor blade spars and fuel pods) [5], automotive and structure applications (e.g., battery trays, seat structures, front end modules and load floors) [6]. However, robust process simulation methods and adaptive design tools are needed to shorten the design cycle and reduce manufacturing cost, creating reliable final products and expanding the applications of textile composites. Some examples of the fundamental questions from practitioners are (1) Is it possible to form a specific three-dimensional geometry without wrinkles or fiber breakage? (2) What are the final fiber orientations? (3) What is the final fiber distribution? (4) What process parameters should be used to form such a part? To answer these questions, an understanding of the mechanical behavior of woven fabric is a key cornerstone.

Recognizing these requirements, a group of international researchers gathered at the University of Massachusetts Lowell for the *Workshop on Composite Sheet Forming* sponsored by the U.S. National Science Foundation in September of 2001. The main objectives of the workshop were to better understand the state of the art and to identify the existing challenges in both materials characterization and numerical methods required for the robust simulations of forming processes. One direct outcome of the workshop, and the effort to move towards standardization of material characterization methods, was a web-based forum exclusively for research on the forming of textile composites, which was established in September 2003 [7]. Other outcomes of the workshop are in the form of publications [8–57], such as this one, highlighting recommended practices for experimental techniques and modeling methods.

Material property characterization and material forming characterization were the two main areas related to material testing identified at the 2001 NSF Composite Sheet Forming workshop. Standard material testing methods are necessary for researchers to understand the formability of the material, the effects of process variables on formability, and to provide input data and validation data for numerical simulations. Thus, the researchers embarked on a benchmarking project to comprehend and report the results of material testing efforts currently in use around the world for textile composites to make recommendations for best practices. Only the benchmark activities on material property characterization are reported in this paper. Benchmark activities on the material forming characterization, modeling methods, and frictional behavior will be reported in future articles.

Three different commingled fiberglass–polypropylene woven composite materials were used in this collaborative effort. The materials were donated by Vetrotex Saint-Gobain in May 2003 and were distributed in July 2003 to the following research groups: Hong Kong University of Science and Technology (HKUST) in Hong Kong, Katholieke Universiteit Leuven (KUL) in Belgium, Laboratoire de Mécanique des Systèmes et des Procédés (LMSP), INSA-Lyon (INSA) in France, Northwestern University (NU) in the USA, University of Massachusetts Lowell (UML) in the USA, University of Twente (UT) in the Netherlands, and University of Nottingham (UN) in the UK.

Intra-ply shear is the most dominant deformation mode in woven composite forming (Fig. 3); therefore, the trellis-frame (picture-frame) test (Fig. 4) and the bias-extension test (Fig. 5) were identified for further study related to material shear-property characterization. Six research groups listed submitted data for the experimental trellising-shear section of the benchmark project and four research groups submitted data for the bias-extension test. A summary and comparison of the test methods and the findings from all participating research groups is presented. The rest of

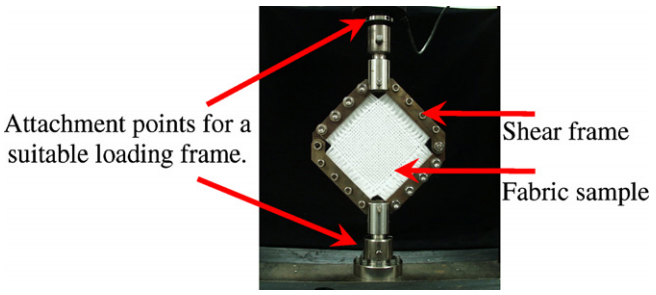

Fig. 4. Trellising-shear test apparatus.

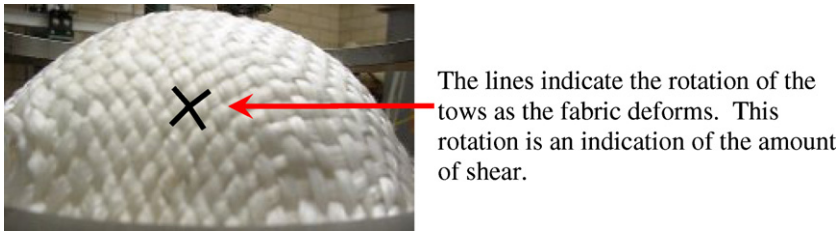

Fig. 3. Fabric shearing.

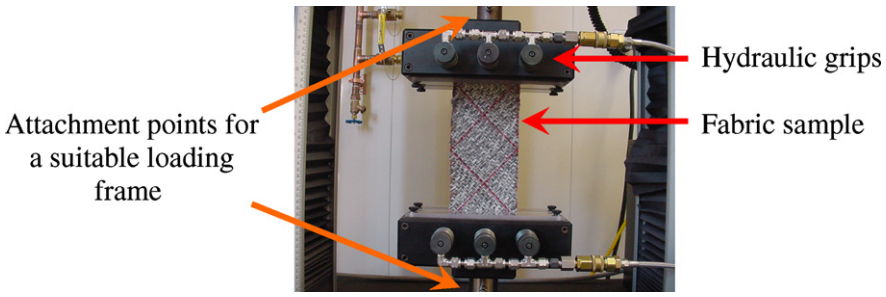

Fig. 5. Bias-extension test apparatus.

this paper is organized as follows: a summary of the properties of the materials used in this study is presented in Section 2, trellis-frame setups at each participating institution and data processing procedures are discussed in Section 3, and trellis-frame test results and the normalization analysis are presented in Section 4. Similarly, the experimental setup procedure and analytical calculation of bias-extension are presented in Section 5, while Section 6 has the results from the bias-extension tests. Finally, the comparison of normalized shear force vs. shear angle obtained from trellis-frame and bias-extension tests is compared in Section 7 followed by a discussion on how the data from these tests can be used to advance the benchmarking effort related to the numerical modeling of the benchmark fabrics in thermo-stamping simulations, and recommended future work.

2. Fabric properties

The three types of woven fabrics used in this study were donated by Vetrotex Saint-Gobain (Fig. 6). The fabric properties, as reported by the material supplier and benchmark participants, are listed in Table 1. Each fabric comprised yarns with continuous commingled glass and polypropylene (PP) fibers. These fabrics were chosen because of their ability to be formed using the thermo-stamping method.

3. Experimental setups of the trellis-frame test

A trellis frame, or picture frame, shown in Fig. 4 is a fixture used to perform a shear test for woven fabrics [58–60]. Fig. 7 shows a fabric sample loaded in a picture frame both in the starting position and also in the deformed position. Using this test method, uniform shearing of the majority of the fabric specimen is obtained. Displacement and load data are recorded to aid in the characterization of pure shear behavior. Because recommendations for best practices and standardized test procedures were two of the desired outcomes of this research, we did not limit all groups to perform the test using exactly the same procedure. However, the tests were equivalent in principle. In all picture-frame tests, the fabric sample

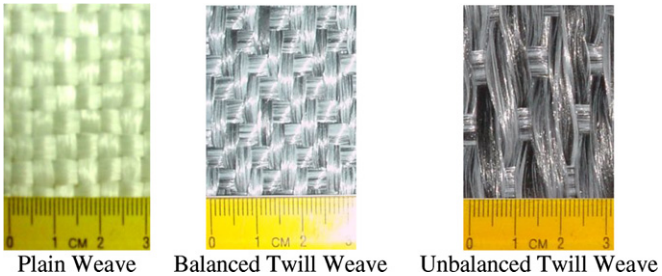

Fig. 6. Woven fabrics used in this study.

Table 1
Fabric parameters (as reported by the material supplier unless specified otherwise)

	Manufacturer's style[a]		
	TPEET22XXX	TPEET44XXX	TPECU53XXX
Weave type	Plain	Balanced twill	Unbalanced twill
Yarns	Glass/PP	Glass/PP	Glass/PP
Weave	Plain	Twill 2/2	Twill 2/2
Area density, g/m^2	743	1485	1816
Yarn linear density, tex	1870	1870	2400
Thickness[b], mm	1.2 (NU)	2.0 (NU)	3.3 (NU)
Yarn count, picks/cm or ends/cm			
Warp	1.91 (KUL) 1.93 (HKUST) 1.95 (NU)	5.56 (KUL)	3.39 (KUL)
Weft	1.90 (KUL) 1.93 (HKUST) 1.95 (NU)	3.75 (KUL)	1.52 (KUL)
Yarn width in the fabric, mm			
Warp	4.18 ± 0.140 (KUL)[c] 4.20 (HKUST) 4.27 (NU)	1.62 ± 0.107[c] (KUL)	2.72 ± 0.38[c] (KUL)
Weft	4.22 ± 0.150 (KUL)[c] 4.20 (HKUST) 4.27 (NU)	2.32 ± 0.401[c] (KUL)	3.58 ± 0.21[c] (KUL)

[a] Designated by Twintex.
[b] ASTM Standard D1777 (applied pressure = 4.14 kPa).
[c] Standard deviation.

is initially square and the tows are oriented in the 0/90 position to start the test (Figs. 7 and 8). By using varying procedures, researchers could study and recommend methods for data comparison.

Before discussing the test procedure in detail, it should be noted that some groups chose not to submit results for all of the fabrics included in this study. Table 2 shows the tested fabrics by each participant.

All researchers reported load histories and global-shear-angle data for picture-frame tests conducted at room temperature. The group decided that even though the temperature effect was an important part of the process, initial comparisons among results obtained using non-standard test procedures should be conducted without varying the temperature. When the differences were understood at room temperature, the additional complexity of comparing results at elevated temperatures would be incorporated into the study. In the remaining paragraphs of this section, frame design and the clamping mechanism, sample preparation, shear angle calculation and shear force calculation will be presented.

3.1. Frame design and clamping mechanism

Fig. 8 illustrates the different frame designs used in five research groups. Although the frames used in this study are not

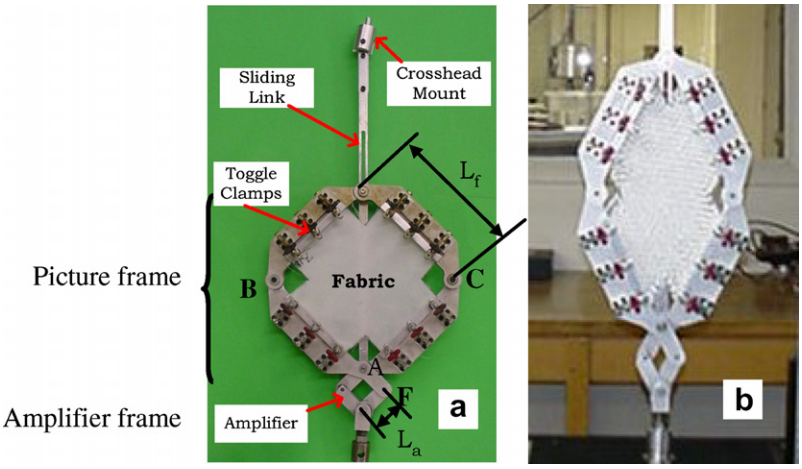

Fig. 7. UML shear frame: (a) starting position and (b) deformed position. (Note that the top hinge has traveled from the bottom of the slot in the undeformed position (a) to the top of the slot in the deformed position (b).)

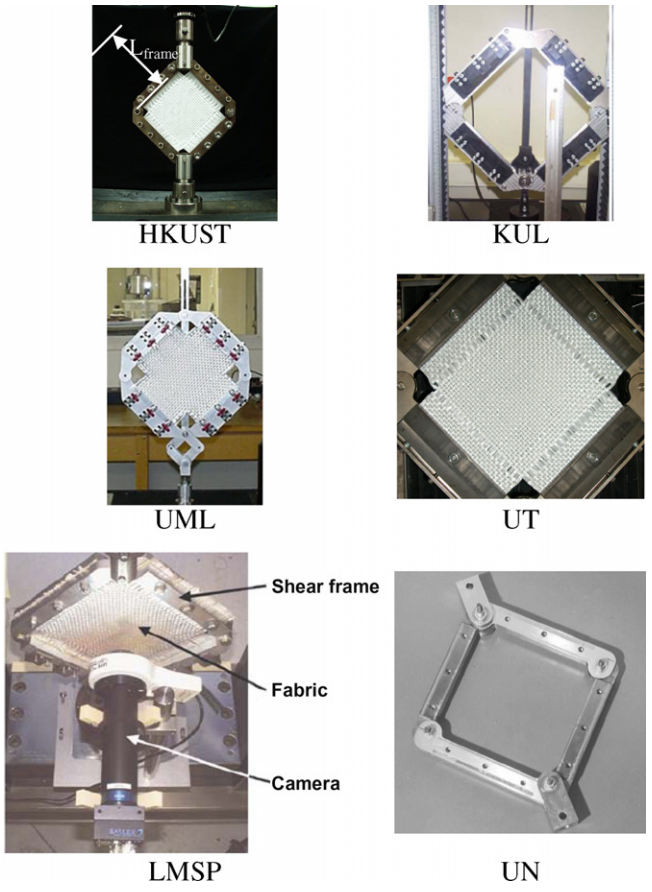

Fig. 8. Picture frames designed, fabricated and used by the research groups.

identical, all of them have common features. For example, the corners of each frame are pinned. When the fabric is loaded into the frame, it is clamped on all edges to prevent slippage. The corners of a sample are cut out to allow the tows to rotate without wrinkling the fabric. Thus, it appears that each sample has four flanges (Fig. 8). It was assumed that all clamping mechanisms held the fabric rigidly in the frame and there was no slippage.[9]

[9] This assumption was later eliminated in the work of Boisse's group [28], in which they found that clamping force plays an important role in the measurement of shear behavior using picture-frame tests.

Table 2
Tested fabrics in picture-frame tests used by participating researchers

Group	Plain weave	Balanced twill weave	Unbalanced twill weave
HKUST	Y	N	N
KUL	Y	Y	Y
LMSP	Y	N	N
UML	Y	Y	Y
UT	Y	Y	N
UN	Y	N	Y

Note: Y = data reported; N = data not reported.

Thus, differences in clamping mechanisms are not taken into account in the analysis of the results, and the friction effect between the fabric and grips can be ignored. With the fabric properly aligned and tightly clamped in the frame, the distance between two opposing corners is increased with the aid of the tensile testing machine, and therefore the tows begin to reorient themselves as they shear (Fig. 7).

Note from Figs. 7–9 the inclusion of a sliding slot in the KUL and UML frames. While the shear frames of HKUST, UT and LMSP were displaced at the opposing two joints of their frames, the mechanism by which the fabric deforms is aided by linkages in the frames used by KUL and UML. UML's linkage was added to allow the frame to displace at a greater speed than that which could be achieved by the tensile test machine alone. It was found that the frame could travel at a rate 4.25 times faster than what was possible through the specified crosshead displacement rate. In addition to amplifying the distance traveled, these linkages amplify the measured force, and this amplification factor must be accounted for when the results from all the groups are analyzed and compared. A detailed discussion of the amplification factor associated with the inclusion of the linkages and the various normalization techniques is included in the discussion of results (Section 4). This section focuses on the similarities and differences of the test methods used by each group.

3.2. Sample preparation

The sample size is noted as the area of the fabric without the flanges because this area represents the amount of fabric that is deformed during the test. It is the area that encompasses the tows which must rotate at the crossover points during the test. Table 3 lists the frame size and the maximum fabric size in one direction and the testing speeds used by different research groups.

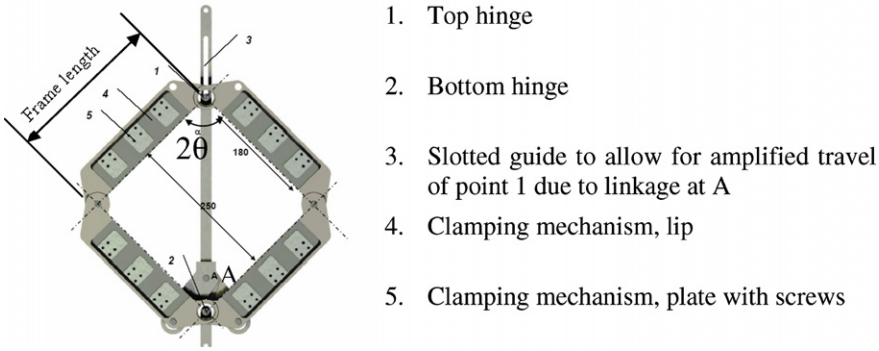

Fig. 9. Schematic of picture frame (KUL).

Table 3
Frame size and test parameters

Group	Frame (mm)	Fabric (mm)	Speed (mm/min)	Specimen temperature
HKUST	180	140	10	Room temperature
KUL	250	180	20	
LMSP	245	240	75–450	
UML	216	140	120	
UT	250	180	1000	
UN	145	120	100	

In addition to the difference in the sample size, additional differences among the groups were related to sample preparation. For example, to eliminate the potential force contribution from shearing of the yarns in the edge (arm) parts of the sample, HKUST removed all of the unclamped fringe yarns (Fig. 10). UT reported that they removed some of the yarns adjacent to the center area of the sample to prevent the material from wrinkling during testing (Fig. 10). In the previous research by Lussier [43], it was reported that care must be taken not to alter the tightness of the weave or local orientation of the remaining yarns when removing some yarns prior to testing the fabric. This statement was further supported by HKUST who noted that theoretically in an obliquely oriented or misaligned specimen in the frame, one group of yarns would be under tension while the other would be under compression. Because a yarn cannot be compressed in the longitudinal direction, a misalignment would indicate that the yarn buckles out of the original plane and the onset of wrinkling in the fabric occurs at lower shear angles than when the specimen is properly aligned in the frame.

UT terminated their tests at the onset of wrinkling, as the shear deformation is no longer uniform once wrinkling occurs. UML noted that by "mechanically conditioning" the specimen, i.e., by shearing the fabric in the frame several times before starting the test, the variability in tension due to local deviations in orientation could be eliminated. This occurrence indicates the importance of the precise handling of both the sample and the test fixture.

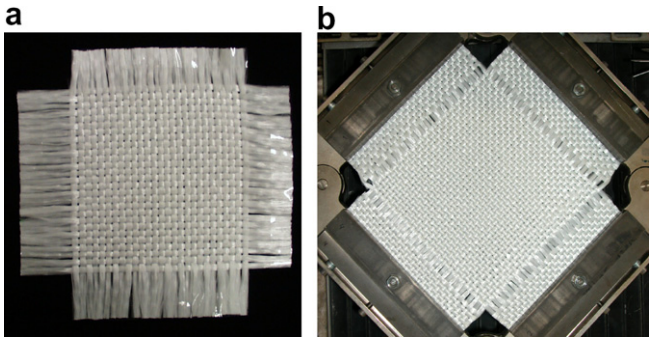

Fig. 10. Specimens with yarns removed from arm regions: (a) HKUST and (b) UT.

3.3. Determination of shear angle

Fabric conforms to its final geometry mostly by yarn rotation, i.e., shearing between weft and wrap yarns, denoted as the shear angle γ. γ is commonly assigned as zero (0) at the initial stage when weft and wrap yarns are perpendicular to each other. We will use this shear angle as a common parameter for comparison in this benchmark activity.

Fig. 8 shows the photos of different frames used in various groups. In the laboratories of HKUST, UT and LMSP, a displacement transducer in the tensile machine measures the vertical displacement, d, of point A. Through trigonometric relations, the angle of the frame, θ, is calculated

$$\cos\theta = \frac{\sqrt{2}L_{\text{frame}} + d}{2 \times L_{\text{frame}}} \tag{1}$$

where L_{frame} is the frame length indicated in Fig. 8. The shear angle, γ, is calculated from the geometry of the picture frame

$$\gamma = 90^\circ - 2\theta \tag{2}$$

This value, γ, is also called the global shear angle. Note that this value is taken to be an average shear value over the entire specimen. The actual shear angle at any point on the fabric may vary.

Figs. 7 and 9 show the picture frames used at UML and KUL, respectively, where both had a linkage in their frames. In this case, the displacements at point A in the corresponding figures are reported. Therefore, instead of L_{frame} in Eq. (1), the length of amplifier link, L_a, as indicated in Fig. 7 was used in Eq. (1) to calculate the angle of the frame. Eq. (2) applied to all five cases.

Optical methods, which can aid in the determination of the shear angle at any particular point on the fabric specimen, also exist. HKUST used a camera to capture the arrays of images during the loading process. They then processed these images with AutoCAD, as shown in Figs. 11 and 12. They found that the maximum deviation between the measured shear angle and the calculated shear angle (Eq. (2)) is about 9.3% and that the maximum deviation typically occurs at larger shear angles.

KUL incorporated an image mapping system (Aramis) into their experiment. After photos were taken by a CCD camera, displacement and strain fields were identified by the Aramis software by analyzing the difference between two subsequent photos. Fig. 13 shows a distribution of the total equivalent strain over an image of a fabric sample during testing. By averaging the local shear angles produced by Aramis and comparing them with the global

Fig. 11. Array of images captured during the loading process (HKUST).

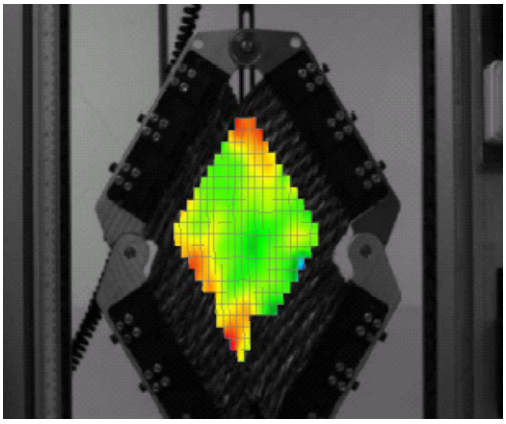

Fig. 13. Image of the fabric and the central region with the von Mises strain field (KUL).

shear angles calculated from the crosshead displacement using Eqs. (1) and (2), KUL generated the graph depicted in Fig. 14, which shows that the shear angle values obtained using the two methods are comparable. However, for the unbalanced twill weave, the difference becomes larger after a shear angle of 33°.

LMSP also incorporated an image mapping system into their experiments. Optical measures were made with a zoom lens that covered the entire specimen area. A typical measured displacement field is shown in Fig. 15 and the equivalent strain field distribution can then be obtained as shown in Fig. 16 [22]. Note that there exists a variation of logarithmic shear strain, ε_{xy}, in the picture-frame specimen. Fig. 17 compares this logarithmic shear strain obtained by optical measure to those given by the frame kinematics. Similar to the findings reported by KUL, the difference between the calculated shear angle and the measured shear angle is negligible before 33°, however, becoming larger as the frame displacement advanced.

As the difference between the global shear angle and the local shear angle is small especially at the initial deformation zone as confirmed by HKUST, KUL and LMSP, the shear angle reported in the rest of this paper is the global one calculated from the crosshead displacement.

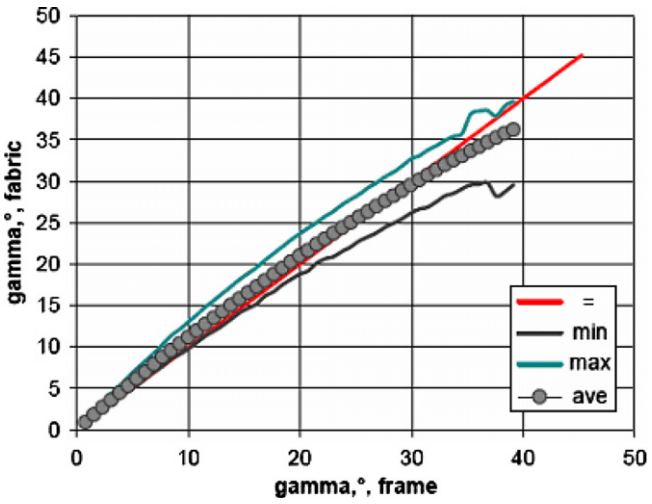

Fig. 14. Typical relationship between the optically measured shear angle and the shear angle of the frame, unbalanced twill weave (KUL).

3.4. Determination of shear force

The force needed to deform the fixture must be measured accurately to determine the actual force required in shearing the fabric. The shear force, F_s, can be calculated from the measured pulling force and the current frame configuration as

$$F_s = \frac{F}{2\cos\theta} = \frac{F'' - F'}{2\cos\theta} \tag{3}$$

where F is the net load and θ is the angle shown in Fig. 9 calculated using Eq. (1). To eliminate the error caused by the weight and inertia of the fixture, the net load F should be obtained by subtracting an offset value F' from the machine-recorded value F'' when the fabric is being deformed in the picture frame.

The offset value F' can be determined by two means. HKUST and UML conducted several tests on their frames without including a fabric sample to record the force required to deform the frame, F'. KUL used a different method to measure the force required to deform the fixture, F'. Their method required a hinge (Fig. 18) to balance the initial weight and calibrate the results under various loading speeds.

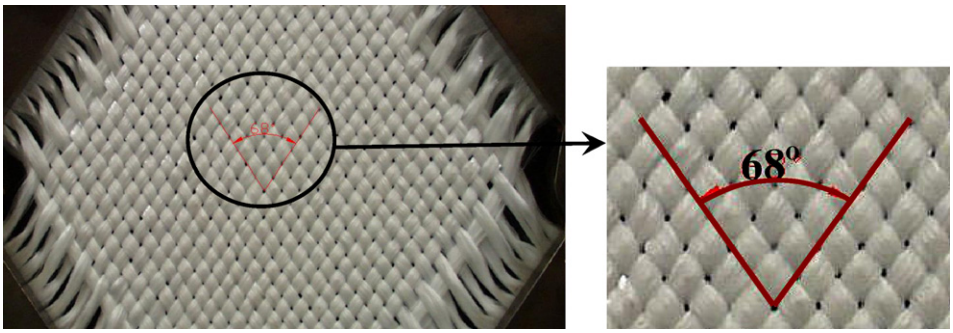

Fig. 12. Shear angle measurement on a photo (HKUST).

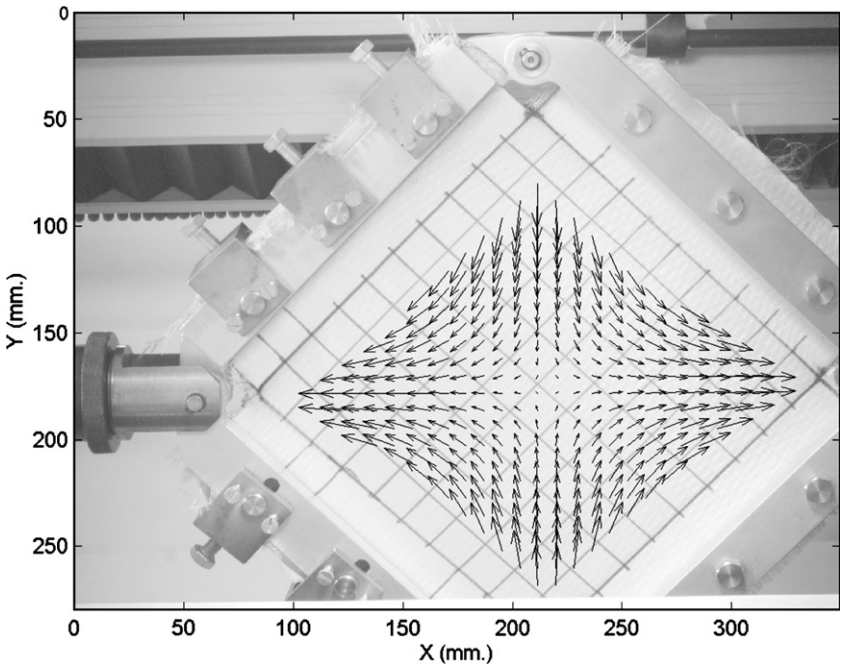

Fig. 15. A typical experimental displacement field of a picture frame measured at LMSP.

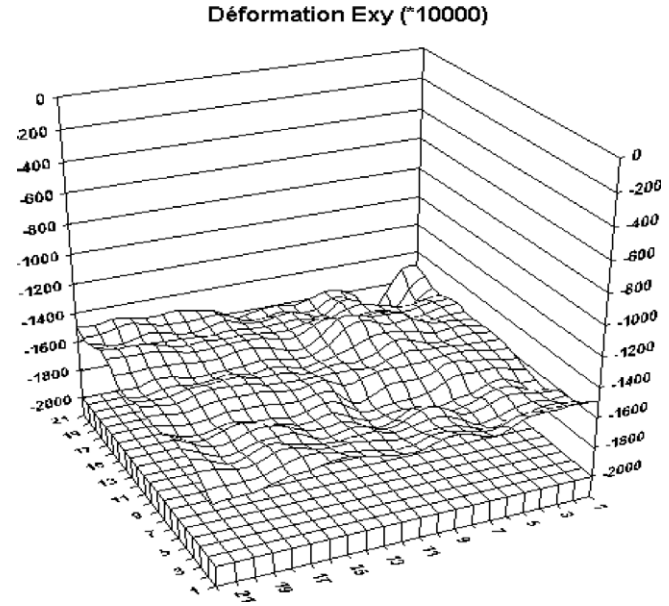

Fig. 16. A typical strain field in a picture-frame test (LMSP).

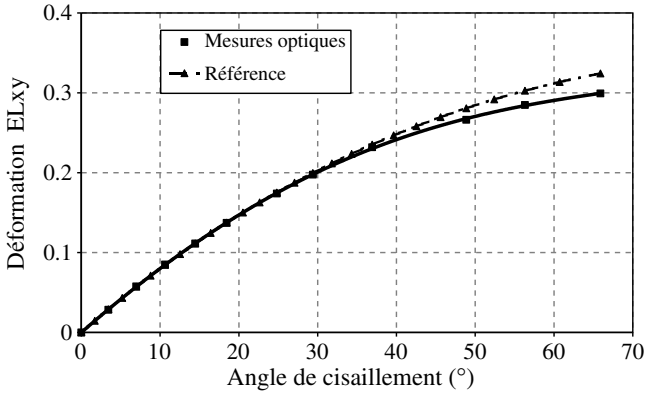

Fig. 17. A comparison between global strain component ε_{xy} measured with optical device and the theoretical strain corresponding to frame kinematics (LMSP).

Recall that UML and KUL have a linkage in their frame design (Figs. 7 and 9), which introduces an amplification factor in the force calculation. To calculate the shear load, the kinematics of the picture frame must be studied.

Let us first examine UML's picture frame shown in Fig. 7. The free body diagrams of the side frame BC and BAF are shown in Fig. 19.

From Fig. 19, note that joint C is free for motion. Using symmetry, it can be determined that the force applied on joint C from links CD and BC is zero. Thus, performing a static analysis using the free body diagram of link BC (Fig. 20a),

$$F_B - F_s = 0 \quad \text{or} \quad F_B = F_s \tag{4}$$

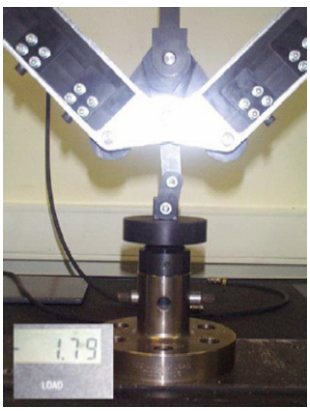

Fig. 18. Hinge for calibrating the force required to deform the frame.

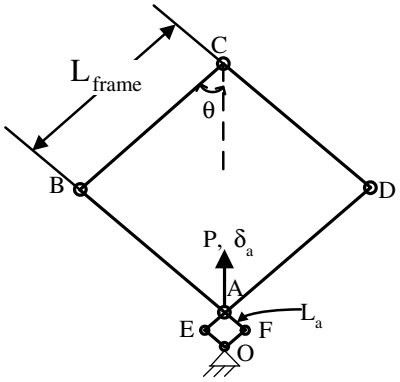

Fig. 19. Schematic diagram of the picture frame at UML.

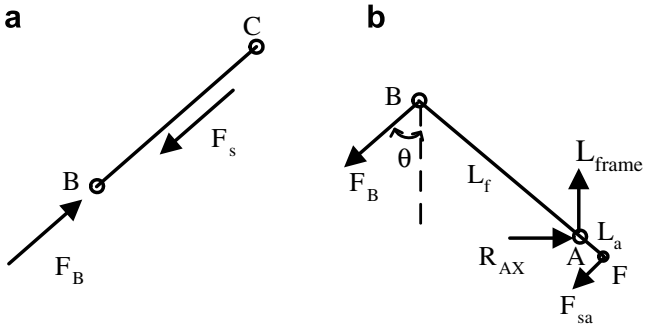

Fig. 20. Free body diagrams of (a) link BC and (b) link BAF.

where F_B is the force on joint B between link BC and link BAF and F_s is the shear force of the fabric sample applied to link BC.

Then, from the free body diagram of link BAF shown in Fig. 20b,

$$M_A = 0 \quad \text{or} \quad F_B L_{frame} \sin(2\theta) - F_{sa} L_a \sin(2\theta) = 0 \tag{5}$$

where M_A is the moment at point A, L_{frame} is the length of link BC, F_{sa} is the shear force applied on the amplifier frame from the tensile machine and θ is the angle between link BC to the vertical direction as seen in Fig. 23. Solving Eq. (5) for F_B,

$$F_B = \frac{F_{sa} L_a}{L_{frame}} \tag{6}$$

Defining an amplification factor as

$$\alpha = \frac{L_{frame}}{L_a} \tag{7}$$

From the geometry of the amplifier frame, the shear force of the amplifier, F_{sa}, can be calculated

$$F_{sa} = \frac{F}{2\cos\theta} \tag{8}$$

where F is the force measured on the load cell in the crosshead or $F' - F'$ in Eq. (3).

Substituting Eqs. (4), (7) and (8) into Eq. (6), we can obtain

$$F_s = \frac{F}{2\alpha\cos\theta} \tag{9}$$

Thus, in processing the picture-frame test data at UML, Eq. (9) is used to calculate the shear load. After comparing Eq. (9) with Eq. (3), it should be noted that the shear force equation is only altered through the inclusion of the amplification factor in the denominator on the right-hand side of the equation. Eq. (9) will reduce to Eq. (3) if the amplification factor, α, approaches 1.

A similar analysis can be performed on the frame used by KUL. However, some differences exist because the amplification linkage in the KUL frame is inverted when compared to the amplification linkage in the UML frame (Figs. 7 and 9). The geometry of the linkage in KUL's frame is shown in detail in Fig. 21. Note that none of the angles of the KUL amplification linkage are equal to the shear angle for the fabric as the crosshead moves in the vertical direction. Thus, the amplification factor for the KUL frame is not a constant value like it was for the UML frame. However, upon performing a kinematic analysis, an equation (as opposed to a constant value) can be determined for the amplification factor, α, and substituted into Eq. (9).

4. Experimental results of the trellis-frame test

In the previous section, frame design, specimen preparation and the calculation of shear angle and shear force were discussed. Here, in this section, results from these six research groups (i.e., HKUST, KUL, LMSP, UML, UT and UN) will be compared. Note that the capacities of the load cells were varied (1–50 kN) from each group. Since the tensile machine with the high load capacity induced noisy load data, the force data were smoothed in advance of the results comparison.

4.1. Behavior of the plain-weave fabric

Fig. 22 shows the data comparison of shear force data by Eq. (9) as a function of the calculated shear angle for plain-weave fabric at room temperature. Here, the amplification factor introduced by the linkages in the frames used at UML and KUL was considered, i.e., L_a was used in the shear angle calculation in Eq. (1) and α was used in

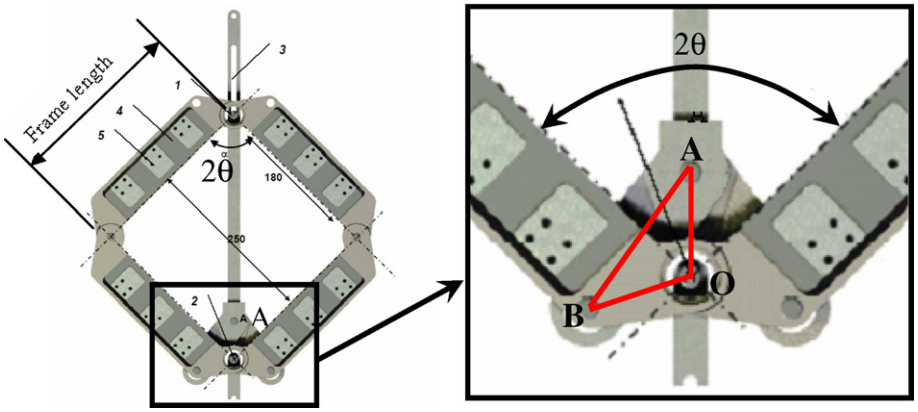

Fig. 21. Geometry of picture frame (KUL).

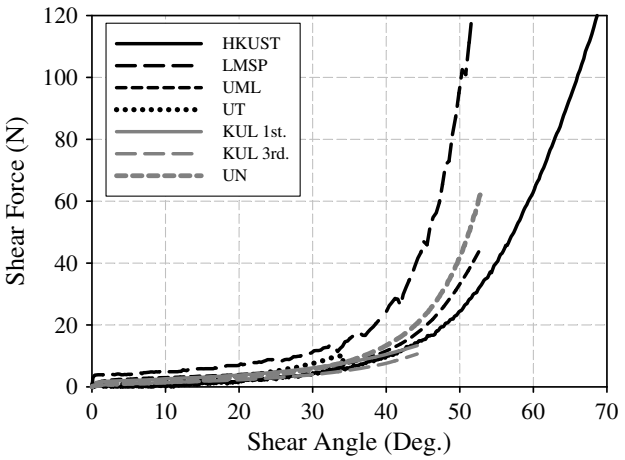

Fig. 22. Shear force vs. shear angle with linkage amplification removed from UML and KUL results.

the shear force calculation in Eq. (9) for data from UML and KUL. In the other cases, L_{frame} was used in Eq. (1) to calculate the shear angles and Eq. (3) was used in obtaining the shear forces. As can be seen from Fig. 22, results show similar behaviors within a certain small angle 35° except for LMSP result. To demonstrate the importance of considering the amplification factor in the calculations, Fig. 23 shows the comparison when the amplification factor was not included, which resulted in a quite different figure. Also, in order to examine how results varied for each data, error bars are plotted in Fig. 23 for several group's curves and the variations in the shear force behavior were below 5 N within a 35° shear angle range.

HKUST and UML mechanically conditioned the samples prior to testing (see discussion in Section 3.2). KUL reported data for each of three repetitions of the test on a single sample. Examining the data from the third repetition of the test on a single sample can be equated to mechanical conditioning, as the sample has deformed two times. KUL noted that the data from the second and third repetitions on a single sample were comparable with each other, but both were below the data from the first time the sample was deformed in the shear frame (see Fig. 23). UT performed their tests using "as is" samples without prior mechanical conditioning, which also explained why their data were slightly higher than the others.

The discussion in the remainder of this subsection will focus on the region of the plot before the shear angle reaches 60°. It is at approximately 45° where locking began to occur for this fabric. Locking refers to the point at which the tows are no longer able to freely rotate and they begin to exert a compressive force on each other as the fabric is further deformed. The force required to deform the fabric begins to increase significantly as the locking angle is reached and surpassed. When the compression of the tows reaches a maximum, wrinkling begins to occur and the fabric begins to buckle out of plane. Wrinkling in a formed part is considered a defect and thus is undesirable. Fig. 24 shows the shear force vs. shear angle obtained from different groups up to 60° of shearing angle where the amplification factor was considered.

Careful readers must have noted one deficiency in the data format presented in Fig. 24, i.e., the total shear force was presented.

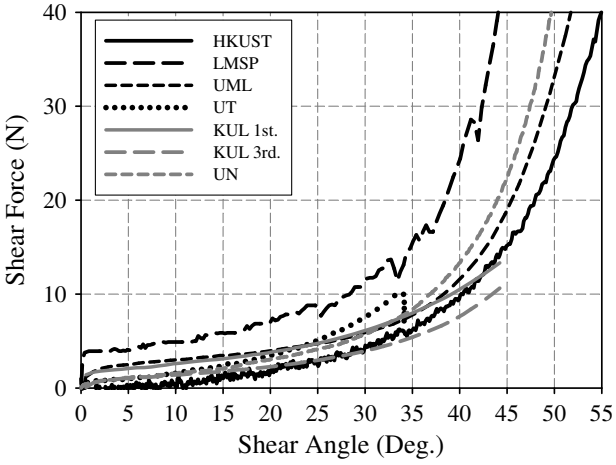

Fig. 24. Shear force vs. shear angle comparison for the plain-weave fabric where the amplification factors in picture frames were considered.

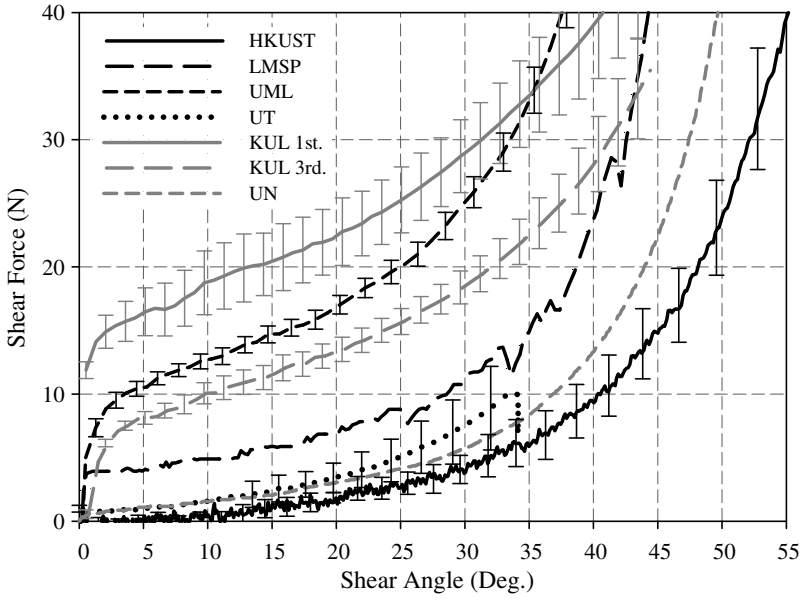

Fig. 23. Shear force vs. shear angle where the amplification factor was not considered.

However, each group has a different frame size as reported in Table 3. One proposed method for normalization was to use the frame length as presented in Harrison et al. [25] based on an energy method. Their assumption was that the frame length was equal to the fabric length. Fig. 25 presents the shear force results normalized by the length of the frame used by each group. As seen, the normalization brought curves closer, but noticeable deviations still exist. Frame length could be an indicative of the sample size, i.e. a larger frame may indicate a larger sample size which in turn would indicate the deformation of a greater number of crossovers. However, as there is no standard ratio for the length of a test sample to the length of the frame, this method is not the best method for normalization.

The investigation continued by comparing the data when normalized by the fabric area. Here, the fabric area was defined as the inner square area of the sample, i.e., the arm areas were neglected as shown in Fig. 26. The fabric area is directly related to the number of crossovers in the material. A larger sample would have more yarns resulting in more crossovers between the yarns. With an increased number of yarns and crossovers, a larger force is required to shear the sample. Fig. 27 shows the results when the data were normalized by the inner fabric area. Again, this normalization technique brought the curves closer together.

The normalization by the inner fabric area is quite straightforward and reasonable if part of yarns in the arm area was pulled out so that no shear occurred in the arm area. However, when yarns in those arm area were not pulled out as shown in Fig. 7, then additional contribution of shear force from the arm area must be considered. Peng et al. [44] proposed a normalization method based on an energy method. They studied the case where the length of the fabric sample was not necessarily equal to the length

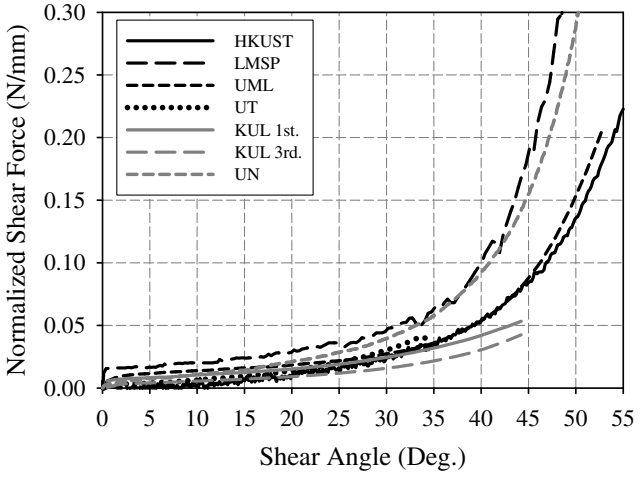

Fig. 25. Shear force normalized by the frame length vs. shear angle.

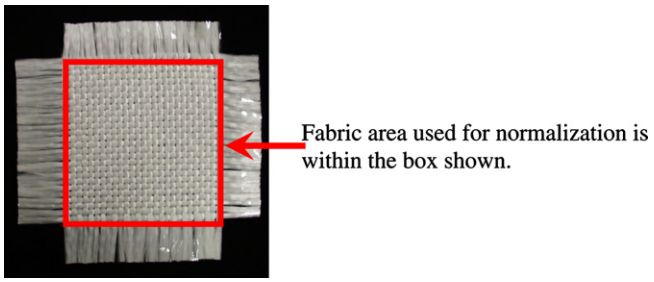

Fig. 26. Sample area used for normalization as shown in Fig. 27.

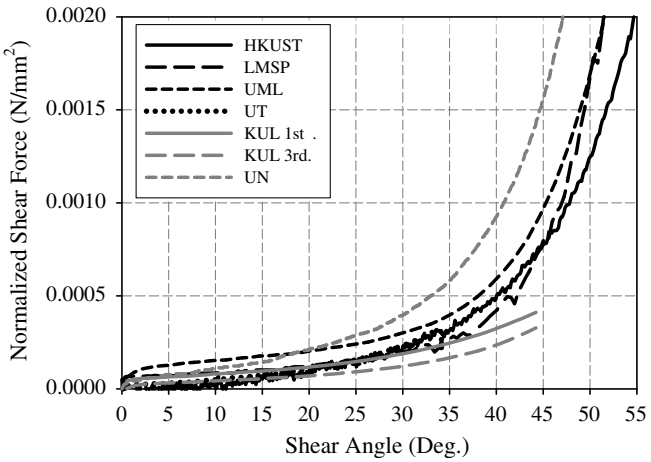

Fig. 27. Shear force normalized by the inner fabric area vs. shear angle.

of the frame. The shear force data can be normalized using the following equation:

$$F_{\text{normalized}} = F_s \cdot \frac{L_{\text{frame}}}{L_{\text{fabric}}^2} \tag{10}$$

where $F_{\text{normalized}}$ is the shear force normalized according to the energy method, F_s is the shear force obtained from Eq. (9), L_{frame} is the side length of the frame and L_{fabric} is the side length of the fabric.

The above equation reduces to the method proposed by Harrison et al. [25] for the case when the fabric length is equal to the frame length, in which case $L_{\text{frame}} = L_{\text{fabric}}$, and

$$F_{\text{normalized}} = F_s \cdot \frac{1}{L_{\text{frame}}} = F_s \cdot \frac{1}{L_{\text{fabric}}} \tag{11}$$

as proposed in Harrison et al. [25]. Fig. 28 presents the normalized data using Eq. (10).

In summary, for the plain-weave fabric tested here, we demonstrated the importance of recognizing different frame designs used in the benchmark and therefore obtaining the correct shear force is the very first step in material characterization. Fig. 22 presents the calculated total shear force vs. the calculated global shear angle in each test where Fig. 24 shows the same data but up to a shear angle of 60° for better illustration. Furthermore, the total shear force is first normalized by only the frame size shown in Fig. 25, by only the inner fabric area shown in Fig. 27 and finally by the combination of frame size and fabric size shown in Fig. 28. From Fig. 28, it can be

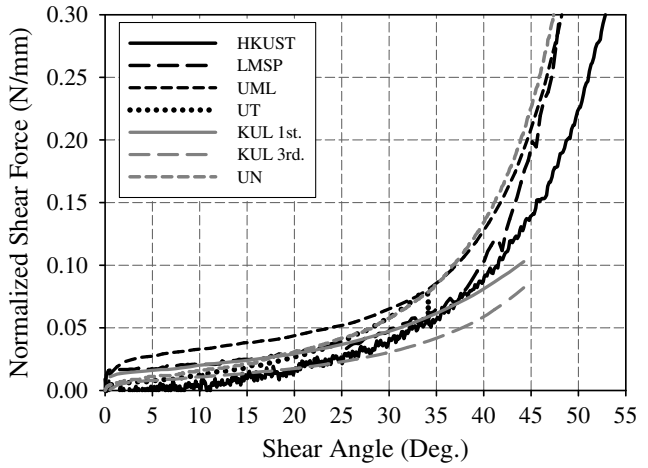

Fig. 28. Shear force normalized using the energy method vs. shear angle.

concluded that the testing results from different groups using different shear frames can be compared for plain-weave fabrics.

4.2. Behavior of the balanced twill-weave fabric

Similarly, picture-frame tests for the balanced 2×2 twill-weave fabric were conducted in KUL, UML and UT as indicated in Table 2. The properties of the fabric are listed in Table 1. Following the same procedure outlined in Section 4.2, here, only the final results of the normalized shear forces using Eq. (10) are plotted against the global shear angle (Eq. (2)) as shown in Fig. 29 considering the amplification factor resulting from the specific shear frame design. Note that the scattering for this fabric is much greater than that of the plain-weave one.

4.3. Behavior of the unbalanced twill-weave fabric

Finally, picture-frame tests for the unbalanced 2×2 twill-weave fabric were conducted in KUL, UML and UN. Due to the relatively large yarn size of this fabric compared to the picture frame and the difficulties of handling this fabric, only two groups submitted their testing results. The properties of the fabric are listed in Table 1. Following the same procedure outlined in Section 4.2, here, only the final results of the normalized shear forces using Eq. (10) are plotted against the global shear angle (Eq. (2)) as shown in Fig. 30 considering the amplification factor resulting from the specific shear frame design. Between these three groups, the comparison is acceptable.

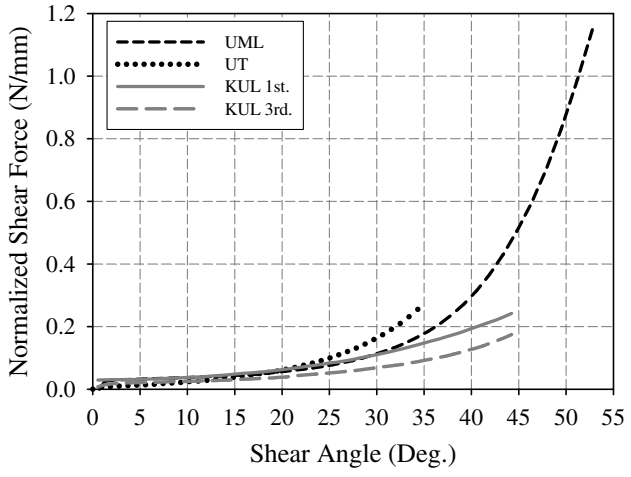

Fig. 29. Normalized shear force vs. global shear angle of the balanced twill-weave fabric.

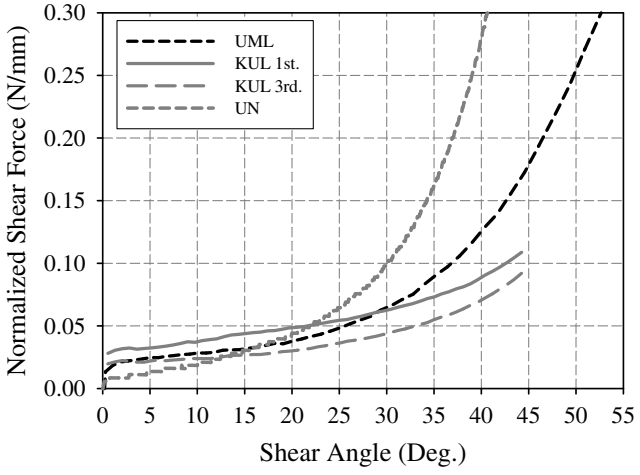

Fig. 30. Normalized shear force vs. shear angle of the unbalanced twill-weave fabric.

5. Experimental setups of the bias-extension test

The bias-extension test involves clamping a rectangular piece of woven material such that the warp and weft directions of the tows are orientated initially at 45° to the direction of the applied tensile direction [25]. Fig. 31 shows a sample set where the specimen is placed in an oven so that high temperature tests could be conducted. In the bias-extension test, when the initial length of the sample (L_0) is more than twice the width of the sample (w_0), there exists a perfect pure shear zone in the center of a sample (zone C shown in Fig. 32). It has been shown [61] that the shear angle in region C is assumed to be twice that in region B, while region A remains undeformed assuming yarns being inextensible and no slip occurs in the sample. Therefore, the bias-extension test is considered to be an alternative to the picture-frame test to study the material behavior of fabrics.

Several research groups conducted the bias-extension tests and reported load histories and global-shear-angle data conducted at room temperature which are listed in Table 4. In the remaining paragraphs of this section, sample preparation, shear angle and shear force calculation will be presented.

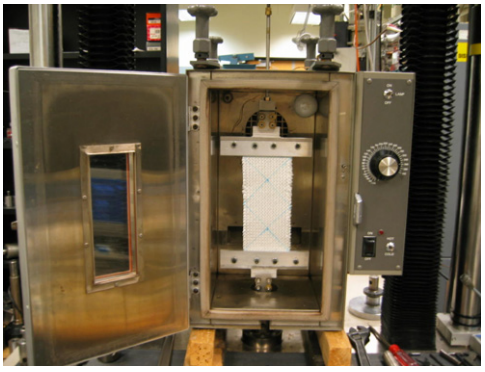

Fig. 31. A bias-extension sample in an oven.

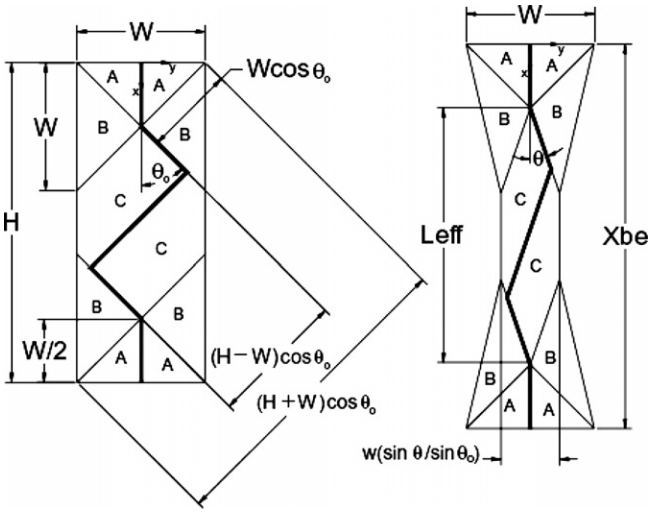

Fig. 32. Illustration of a fabric specimen under a bias-extension test [61].

Table 4
Tested fabrics in bias-extension tests used by participating researchers

Group	Plain weave	Balanced twill weave	Unbalanced twill weave
HKUST	Y	N	N
INSA-Lyon/NU	Y	Y	Y
NU	Y	Y	N
UN	Y	N	Y

Note: Y = data reported; N = data not reported.

5.1. Sample preparation

Unlike the picture-frame tests, the clamping device and sample preparation in bias-extension tests are much simpler. Take NU's tests for example, a pair of grippers can be easily fabricated as shown in Fig. 33. One critical aspect in the bias-extension test is to ensure that fiber yarns are oriented at ±45° to the edges of the grippers before testing. As shown in Fig. 34, for an unbalanced weave, extra care must be given. The black solid lines indicate the fiber yarn directions while an initial visual inspection might wrongly take the dashed lines as initial fiber yarn directions. A twist of fabric might be noticed in the bias-extension test if the initial fiber yarn directions are not orientated exactly.

An aspect ratio of two (2) was used to prepare samples at HKUST, NU, UN and INSA-Lyon/NU. Lines were drawn from the central point of the sample's edge at A to point B along the warp yarn and through other points as depicted in Fig. 35, which shows a marked plain woven fabric with a yarn width of 4 mm. These lines would be used to help measure the shear angle variation during the test. The areas of CIGJ and KHLF are clamped by the grippers. Setting the initial length precisely helps to improve the repeatability of tests. When the sample is under loading, the extension, the tensile force, the width of the sample in the middle, and the angles between DE and EA, and the angle between HE and EF can be recorded. For samples using other aspect ratios, one can prepare a mold to copy the pattern onto the fabric. Table 5 lists the sample sizes and process conditions used in various groups.

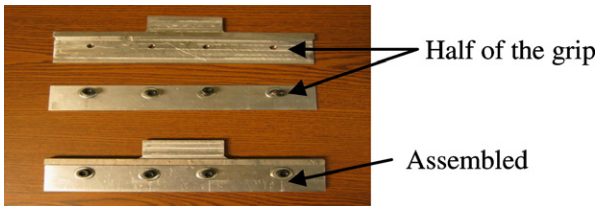

Fig. 33. A picture of the grips used at NU's bias-extension tests.

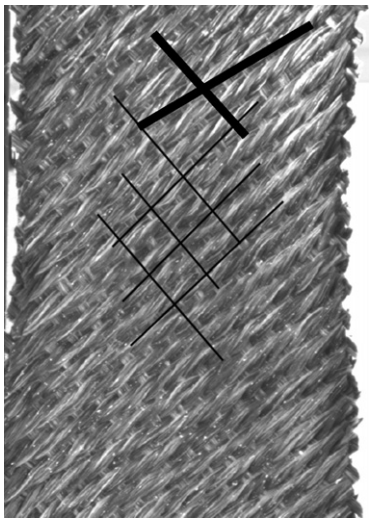

Fig. 34. The unbalanced twill weave fabric in a bias-extension test. Note that the thin solid lines, not the thick solid lines, followed the yarn directions (INSA-Lyon/NU).

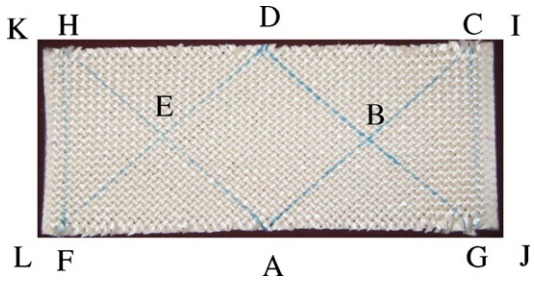

Fig. 35. A 16-yarn sample.

5.2. Determination of shear angle

For a general bias-extension test, Lebrun et al. [61] developed formulae to calculate the global shear angle based on the assumption that there exists three distinguished areas in terms of shear deformation and each area has a uniform shear deformation. Fig. 32 illustrates the notations used in Eq. (12) to calculate the global shear angle

$$\cos\theta = \frac{(H+\delta)-W}{2(H-W)\cos\theta_0} = \cos\theta_0 + \frac{\delta}{2(H-W)\cos\theta_0} \tag{12}$$

where δ is a displacement during the test.

The shear angle in region C (Fig. 32) can also be measured using image processing software based on pictures taken during a test. A joint effort between researchers at INSA-Lyon and NU was made to investigate bias-extension tests. The true shear angle in the fabric was measured using two methods. The solid line with triangle symbols shown in Fig. 36 was the result from the manual measurements of angles based on the images taken. The solid line with square symbols was the result from the image correlation software, IcaSoft developed at INSA-Lyon [62,63]. As can be seen, the shear angle from the software showed a good agreement with the actual (measured) shear angle. Furthermore, it was concluded that the theoretical shear angle calculated by Eq. (12), represented

Table 5
Sample size and process condition used in the bias-extension tests

Group	Material	Length (mm)	Width (mm)	Speed (mm/min)	Temperature (°C)
HKUST	Plain weave	230	115	10	20
INSA-Lyon/NU	Plain weave	230	115		
		300	100		
		450	150		
	Balanced twill weave	300	150		
		300	100		
		450	150		
	Unbalanced Twill weave	400	200		
NU-new	Plain weave	230	115		
NU-old	Balanced twill weave	240	120		
		300	150		
UN	Plain weave	200	100	50	
		250	100		
		300	100		
	Unbalanced twill weave	200	100		
		250	100		
		300	100		

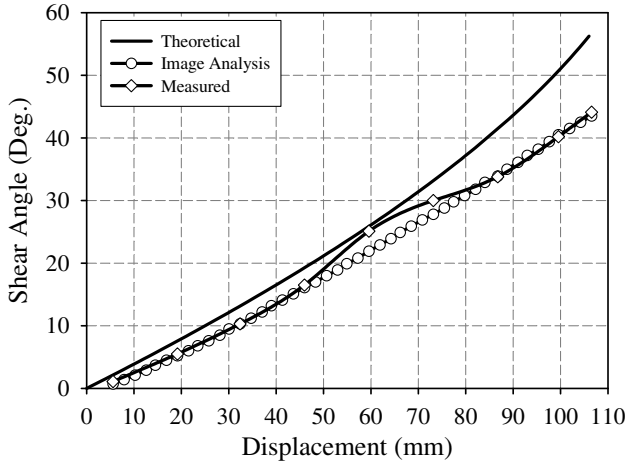

Fig. 36. Plot of shear angle in zone C vs. displacement of the plain weave fabric with a sample size of 150 mm × 450 mm in a bias-extension test (INSA-Lyon/NU).

by the solid black line, can accurately reflect the true shear angle in the fabric until the shear angle reaches a value of 30°. In Fig. 36, the shear angle curves from the image analysis and by manual measurement are compared with the theoretical one for the plain weave with a 150 mm × 450 mm dimension. Note that the difference between the theoretical shear angle and the true shear angle was below 5° until 30° shear angle and became large after this angle. Similar behavior was observed for other fabrics.

The optical measurement was also used to examine another assumption used in the calculation of bias-extension test, i.e., the shear angle in zone B (Fig. 32) is half of that in zone C. Fig. 37 shows a contour of shear angle in a plain weave fabric with a sample size used in a bias-extension test. The contour was obtained from the optical measurement software Icasoft at INSA-Lyon. It can be seen that the assumption held well for the majority of areas.

5.3. Determination of shear force

As discussed in Section 5.2 and illustrated in Figs. 32 and 37, there exists three distinguished deformation zones in a bias-extension test. In this subsection, we will illustrate how to obtain the normalized shear force vs. shear angle from a bias-extension test following the four basic assumptions: i.e., (a) shear angles in each zone are considered uniform; (b) the shear angle in zone C is twice that in zone B; (c) there is no shear deformation in zone A; and (d) the initial fabric has a perfect orthogonal configuration, i.e., $\theta_0 = 45°$.

A simple kinematic analysis of a bias-extension sample shown in Fig. 32 gives us the shear angle in zone C, γ, as a function of fabric size and the end displacement, δ, as

$$\gamma = 90^\circ - 2\theta = 90^\circ - 2\cos^{-1}\left(\frac{L_{\text{eff}}}{\sqrt{2}L_0}\right) = 90^\circ - 2\cos^{-1}\left(\frac{L_0+\delta}{\sqrt{2}L_0}\right) \tag{13}$$

where $L_0 = H - W$ and H and W are the original height and width of the specimen, respectively.

The power made through the clamping force, F, is dissipated in two zones, zone B and zone C

$$F\cdot\dot{\delta} = (C_S(\gamma)\cdot A_\gamma\cdot\dot{\gamma}) + \left(C_S\left(\frac{\gamma}{2}\right)\cdot A_{\frac{\gamma}{2}}\cdot\frac{\dot{\gamma}}{2}\right) \tag{14}$$

where A_γ is the original area of zone C, which is subjected to a shear angle of γ, $A_{\frac{\gamma}{2}}$ is the original area of zone B, and $C_S(\gamma)$ is the torque per original unit area that is needed to deform the fabric in shear [64].

From Eq. (13), we can obtain

$$\dot{\gamma} = -2\dot{\theta} = \frac{\sqrt{2}}{L_0\sin\theta}\dot{\delta} \tag{15}$$

Substitute Eq. (15) and geometrical parameters of $A_\gamma = \frac{2HW-3W^2}{2}$ and $A_{\frac{\gamma}{2}} = W^2$ into Eq. (14), we can obtain

$$C_S(\gamma) = \frac{1}{2H-3W}\left(\frac{\sqrt{2}}{W}(H-W)F\sin\theta - W\cdot C_S\left(\frac{\gamma}{2}\right)\right) = \frac{1}{2H-3W}\left(\left(\frac{H}{W}-1\right)F\left(\cos\frac{\gamma}{2}-\sin\frac{\gamma}{2}\right) - W\cdot C_S\left(\frac{\gamma}{2}\right)\right) \tag{16}$$

The unit torque $C_S(\gamma)$ can be related to shear force F_{sh} as

$$C_S(\gamma) = F_{sh}(\gamma)\cdot\cos(\gamma) \quad \text{and} \quad C_S\left(\frac{\gamma}{2}\right) = F_{sh}\left(\frac{\gamma}{2}\right)\cdot\cos\left(\frac{\gamma}{2}\right) \tag{17}$$

Hence,

$$F_{sh}(\gamma) = \frac{1}{(2H-3W)\cos\gamma}\left(\left(\frac{H}{W}-1\right)\cdot F\cdot\left(\cos\frac{\gamma}{2}-\sin\frac{\gamma}{2}\right) - W\cdot F_{sh}\left(\frac{\gamma}{2}\right)\cos\frac{\gamma}{2}\right) \tag{18}$$

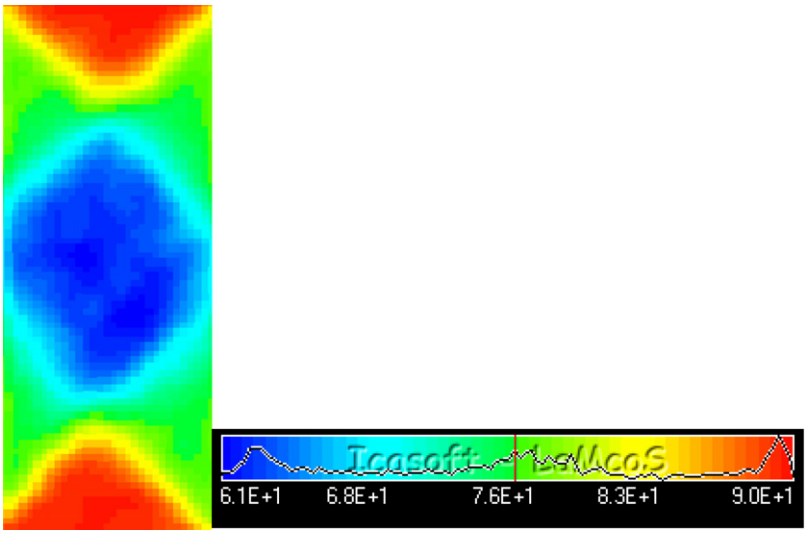

Fig. 37. Contour of shear angle in a plain weave fabric with a sample size in a bias-extension test obtained from the optical measurement software Icasoft (INSA-Lyon/NU).

The above derivation can also be found in [28]. Note that here F_{sh} is the normalized shear force per unit length, the same quantity as $F_{normalized}$ in Eq. (10) from the picture-frame test. Therefore, the experimental clamping force vs. displacement curve can be first converted to the curve of clamping force vs. shear angle using Eq. (12), then using an iterated process, the normalized shear force per unit length F_{sh} can be represented against the shear angle.

6. Experimental results of the bias extension

In the previous section, specimen preparation and the calculation of shear angle and shear force were discussed. Here, in this section, results from four research groups (i.e., HKUST, INSA-Lyon, NU, and UN) will be compared for tests conducted at room temperature. Data labeled as HKUST, NU-old and UN were obtained in 2004, while NU-new was tested in 2007. INSA-Lyon and NU collaborated in the summer of 2007 in performing those tests marked by 'INSA-NU'. UT also submitted their testing data; however, it was for consolidated fabric [12] and therefore will not be included here in this paper. Like the picture-frame test, the force data were smoothed for the highly noised load data.

6.1. Behavior of the plain-weave fabric

Fig. 38 illustrates the raw experimental data with error bars reported from each group. Note that the specimen sizes and ratios are different among those tests. Using Eqs. (12) and (18), normalized shear forces per unit length are plotted in Fig. 39.

As shown in Fig. 39, all data showed consistent results within a certain shear angle 35° range except for 100×200 UN and 100×300 INSA-NU data. The difference might be due to the handling of specimen. Note that the normalized shear force curves were almost similar regardless of the different ratio of width-length and showed good agreement with the results from the picture-frame tests as shown in Fig. 45, which will be discussed in the next section.

Fig. 40 shows the comparison between high temperature tests and room temperature ones as well as between two different loading speeds. One can clearly see that the tensile load is much lower when the temperature increases. Experiments at high temperature are conducted by heating the sample in an oven to the expected processing temperature before the test (Fig. 31). During the test, the oven is maintained at a specified temperature. As for the loading speed, it can be seen that the deformation rate does not affect the tensile force.

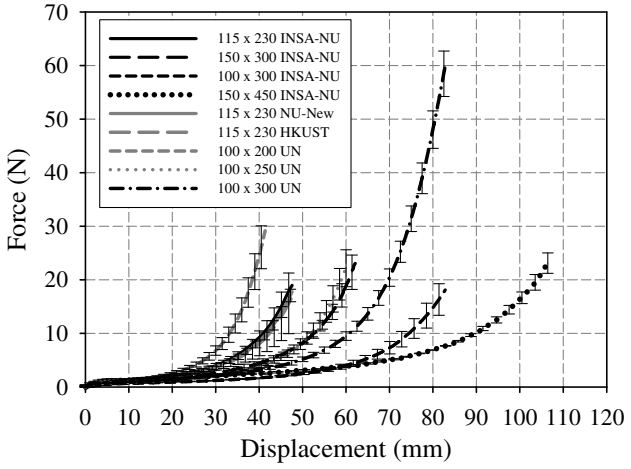

Fig. 38. Tensile force vs. crosshead displacement of plain weave for bias-extension tests.

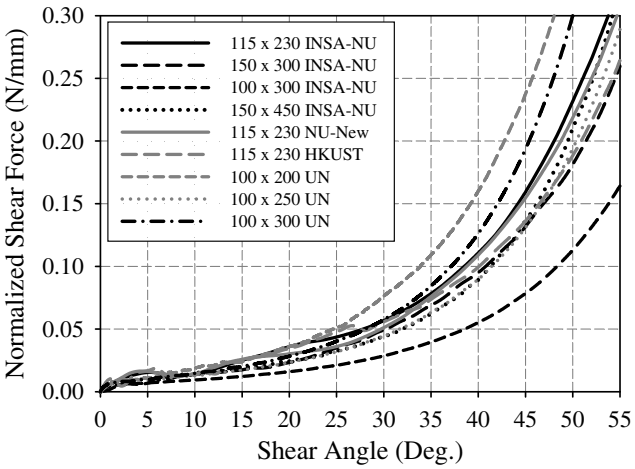

Fig. 39. Normalized shear force obtained from bias-extension tests for plain weave.

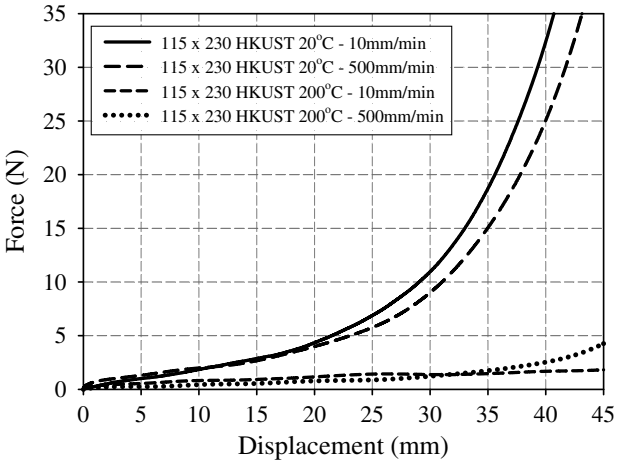

Fig. 40. Load vs. displacement curves of plain weave for high–low temperature and high–low loading speed (HKUST).

6.2. Behavior of the balanced twill-weave fabric

Similarly, the balanced twill-weave fabric was tested at different laboratories. Fig. 41 illustrates the raw experimental data reported from each group. Note that the specimen sizes and ratios are different. Using Eqs. (12) and (18), normalized shear forces per unit length are plotted in Fig. 42. Even several curves showed similar behavior for the normalized shear force, and they still showed a large deviation between each other. However, when the data are compared with the results from the picture-frame tests, the bias-extension results are within the range of the picture-frame test results as shown in Fig. 46.

6.3. Behavior of the unbalanced twill-weave fabric

For the unbalanced twill-weave fabric, only INSA-NU and UN groups reported the test result for the bias-extension test. Both groups performed four tests for each dimension and all results showed almost similar behavior. In Fig. 43, raw experimental data are illustrated. Using Eqs. (12) and (18), the normalized shear forces per unit length are plotted in Fig. 44. Even though the dimension of samples is different from each other, three UN data showed similar behavior while INSA-NU data showed big deviation from UN data.

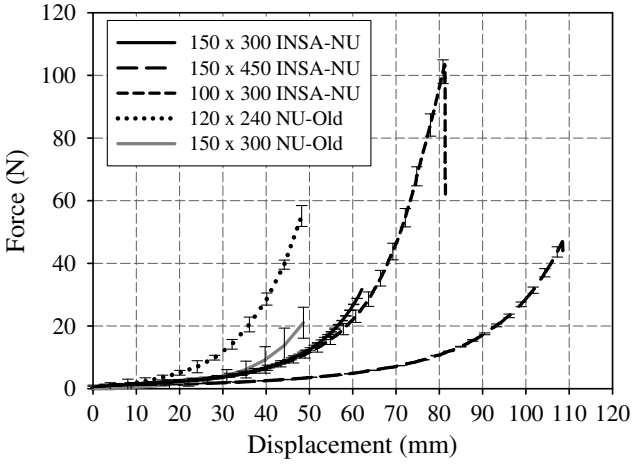

Fig. 41. Tensile force vs. crosshead displacement of balanced twill weave for bias-extension tests.

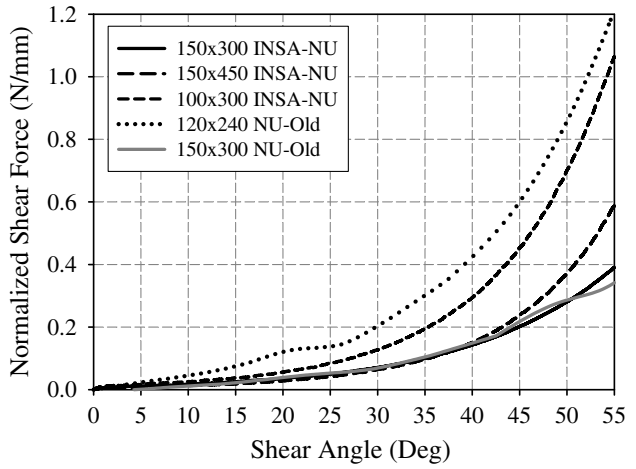

Fig. 42. Normalized shear force obtained from bias-extension tests for balanced twill weave.

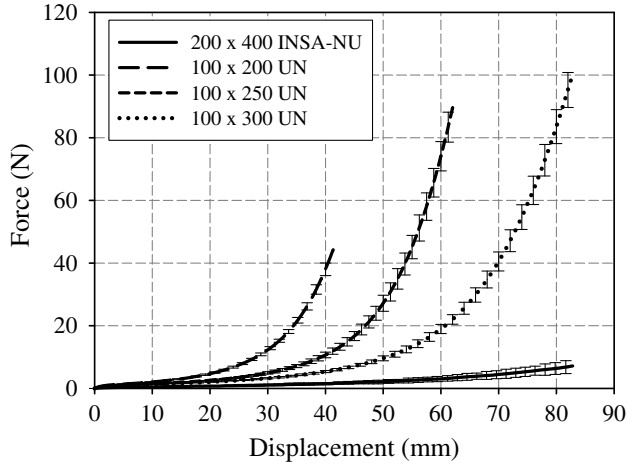

Fig. 43. Tensile force vs. crosshead displacement of unbalanced twill weave for bias-extension tests.

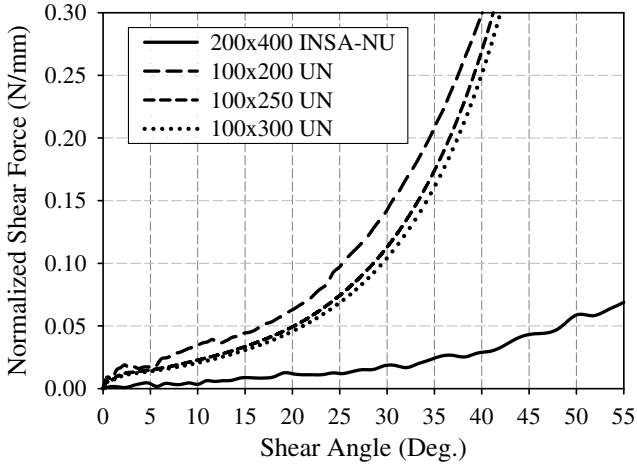

Fig. 44. Normalized shear force obtained from bias-extension tests for unbalanced twill weave.

7. Summary and future work

The properties of woven fabrics are very different from conventional materials, such as bulk metals and polymers. This phenomenon leads to the interest in the material community of woven-fabric composites to conduct benchmark tests. It has been shown that picture-frame tests are able to produce valuable experimental data for characterizing the shear behavior of textile composites. Mechanically conditioning the sample can also improve repeatability as demonstrated in the laboratories. This was shown through results from UML and KUL. UML's samples were all mechanically conditioned and appeared very repeatable. While KUL did not mechanically condition their samples, they conducted the shear test three times on each fabric blank and noted a large difference between the 1st run and the 2nd and 3rd runs. However, there was no large difference in the results when only comparing the 2nd and 3rd runs. Mechanical conditioning may equalize tow tensions left in the fabric from the weaving process and therefore reduces the variability and increases the repeatability. However, mechanical conditioning might not be feasible in industry unless the material handling system is modified.

The optical methods showed that determining the shear angle mathematically from the crosshead displacement was a reasonable method before the plain-weave fabric reaches the 35° shear angle in picture-frame tests and 30° in the bias-extension tests. Therefore, data beyond these angles are recommended to be interrupted using optical measurements instead of theoretical calculation of the shear angle.

Normalization methods were presented for comparing test data from various groups. Now it is interesting to compare the normalized shear force vs. shear angle from picture-frame tests and bias-extension tests. Figs. 45–47 show the comparison results where results from bias-extension tests are in solid curves while those from picture-frame tests are in dash-dotted curves. As shown in Fig. 45, test data showed similar behaviors, even though the testing method and aspect ratios were different. For the balanced twill weave, both test results were located within the same range as shown in Fig. 46, even though the deviation was not small. Therefore, it can be concluded that the suggested normalization methods by Eqs. (10), (12) and (18) for picture-frame and bias-extension tests give consistent shear force behavior for isotropic and homogeneous fabrics. As for the unbalanced twill weave in which the anisotropy and directionality are quite large, both normalization methods did not give consistent results as shown in Fig. 47.

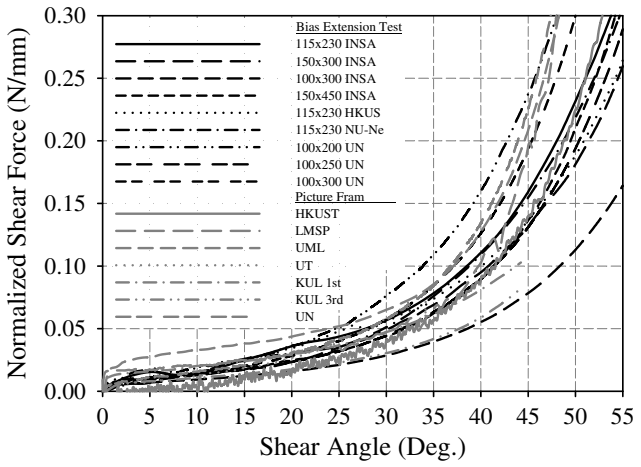

Fig. 45. Normalized shear force vs. shear angle from picture-frame tests and bias-extension tests for plain-weave.

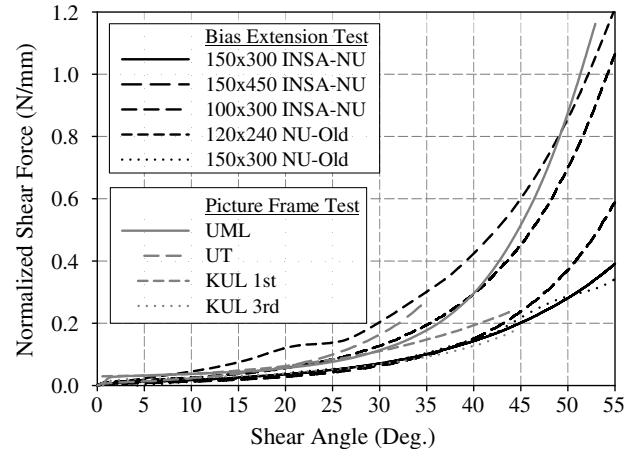

Fig. 46. Normalized shear force vs. shear angle from picture-frame tests and bias-extension tests for balanced-twill weave.

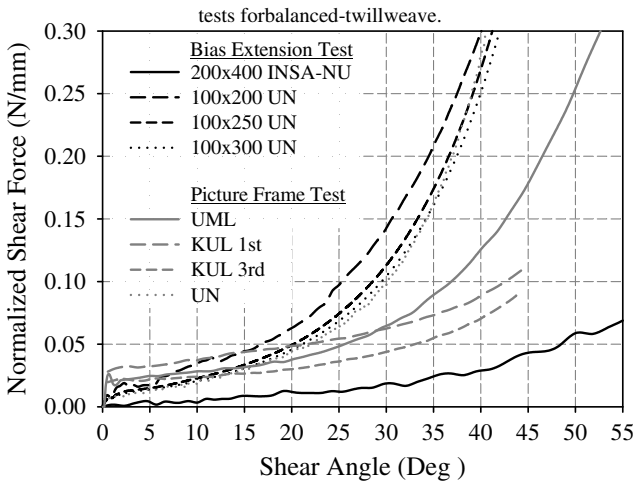

Fig. 47. Normalized shear force vs. shear angle from picture-frame tests and bias-extension tests for unbalanced-twill weave.

Test results provided by different groups show consistency but still have some deviations. Further studies are under way to help develop a standard test setup and procedure for obtaining accurate and appropriate material properties. For example, the effect of clamping force on shear behavior in the picture-frame tests needs to be taken into account in material characterization. Material responses under different speeds and temperatures will be further investigated. Calibration, sample preparation, and other important techniques to increase the accuracy of the tests will be collected and shared among the community. High temperature tests present challenges to researchers as they limit the use of optical devices and require higher sensitivity of the testing equipment.

Since precise descriptions for mechanical material properties in the numerical simulations are required to predict the accurate responses for the composite sheet forming, the well-defined normalization methods are necessary. Even though there still are deviations, the suggested normalization methods can give consistent shear behaviors especially for the homogeneous fabrics. Therefore, further numerical simulations are needed to use the suggesting normalized shear property in order to obtain the consistent forming results and predictions. For the non-homogeneous fabrics such as an unbalanced twill weave, a careful material description is required and further studies for the standardization methods are needed to be investigated. The next phase of this benchmark activity is to focus on the predictability of various material models and simulation methods in modeling the thermo-stamping of woven composites in terms of shear angle prediction, force and deformed shape predictions. Interested readers can refer to the benchmark website [7] for the latest updates.

Acknowledgements

The authors would like to thank the National Science Foundation, Saint-Gobain, Inc., Hong Kong RGC (under Grant HKUST6012/02E), the Netherlands Agency for Aerospace Programmes, a Marie Curie Fellowship of the EC (HPMT-CT-2000-00030) and Engineering and Physical Sciences Research Council (under Grant GR/R32291/01) for their support to this work.

References

[1] Advani SG. Flow and rheology in polymeric composites manufacturing. Amsterdam: Elsevier; 1994.
[2] Parnas RS. Liquid composite molding. Munich: Hanser Publishers; 2000.
[3] Hivet G. Modelisation mésoscopique pour le comportement et la mise en forme des renforts de composites tissés. PhD thesis, University of Orléans; 2002 [in French].
[4] Yu TX, Tao XM, Xue P. The energy-absorbing capacity of grid-domed textile composites. Compos Sci Technol 2000;60(5):785–800.
[5] Rudd CD, Turner MR, Long AC, Middleton V. Tow placement studies for liquid composite moulding. Compos Part A: Appl Sci Manuf 1999;30(9):1105–21.
[6] Long AC, Wilks CE, Rudd CD. Experimental characterisation of the consolidation of a commingled glass/polypropylene composite. Compos Sci Technol 2001;61(11):1591–603.
[7] http://www.nwbenchmark.gtwebsolutions.com/.
[8] Stören Sigurd, editor. ESAFORM 2004, Proceedings of the 7th ESAFORM conference on material forming, Trondheim, Norway, April 27–30, 2004. ISBN: 82-92499-02-04.
[9] Banabic D, editor. ESAFORM 2005, Proceedings of the 8th ESAFORM conference on material forming, Cluj-Napoca, Romania, April 27–29, 2005. ISBN: 973-27-1174-4.
[10] Juster N, Rosochowski A, editors. ESAFORM 2006, Proceedings of the 9th ESAFORM conference on material forming, Glasgow, United Kingdom, April 26–28, 2006. ISBN: 83-89541-66-1.
[11] Cueto E, Chinesta F, editors. ESAFORM 2007, Proceedings of the 10th ESAFORM conference on material forming, Zaragoza, Spain, April 18–20, 2007, ISBN: 978-0-7354-0414-4.
[12] Cao J, Cheng HS, Yu TX, Zhu B, Tao XM, Lomov SV, et al. A cooperative benchmark effort on testing of textile composites. In: ESAFORM 2004; 2004. p. 305–8.
[13] Akkerman R, Lamers EAD, Wijskamp S. An integral model for high precision composite forming. Eur J Comput Mech 2006;15(4):359–77.
[14] Akkerman R, Ubbink MP, De Rooij MB, Ten Thije RHW. Tool-ply friction in composite forming. In: Proceedings of the 10th international ESAFORM conference on material forming, Zaragoza, Spain. AIP conference proceedings, vol. 907; 2007. p. 1080–5.

[15] Badel P, vidal-sallé E, Boisse P. Computational determination of in plane shear mechanical behaviour of textile composite reinforcements. Comput Mater Sci 2007;40:439–48.
[16] Boisse P, Zouari B, Daniel JL. Importance of in-plane shear rigidity in finite element analyses of woven fabric composite preforming. Compos Part A: Appl Sci Manuf 2006;37:2201–12.
[17] Boisse P. Meso-macro approach for composites forming simulation. Int J Mater Sci 2006;41:6591–8.
[18] Boisse P, Gasser A, Hagege B, Billoet JL. Analysis of the mechanical behaviour of woven fibrous material using virtual tests at the unit cell level. Int J Mater Sci 2005;40:5955–62.
[19] Boisse P, Zouari B, Gasser A. A mesoscopic approach for the simulation of woven fibre composite forming. Compos Sci Technol 2005;65:429–36.
[20] Cao J, Xue P, Peng XQ, Krishnan N. An approach in modeling the temperature effect in thermo-forming of woven composites. Compos Struct 2003;61(4):413–20.
[21] Cheng HS, Cao J, Mahayotsanun N. Experimental study on behavior of woven composites in thermo-stamping under nonlinear temperature trajectories. Int J Forming Process 2006;8:1–12.
[22] Dumont F, Hivet G, Rotinat R, Launay J, Boisse P, Vacher P. Field measurements for shear tests on woven reinforcements. Mécanique Ind 2003;4:627–35.
[23] Gorczyca Jennifer, Sherwood James, Liu Lu, Chen Julie. Modeling of friction and shear in thermo-stamping process—Part I. J Comp Mater 2004;38:1911–29.
[24] Harrison P, Lin Hua, Ubbink Mark, Akkerman Remko, van de Haar Karin, Long Andrew C. Characterising and modelling tool-ply friction of viscous textile composites. In: Proceedings of the 16th international conference on composite materials, Kyoto, Japan, ICCM-16; 2007.
[25] Harrison P, Clifford MJ, Long AC. Shear characterization of viscous woven textile composites: a comparison between picture frame and bias extension experiments. Compos Sci Technol 2004;64:1453–65.
[26] Hivet G, Boisse P. Consistent 3D geometrical model of fabric elementary cell. Application to a meshing preprocessor for 3D finite element analysis. Finite Elem Anal Des 2005;42:25–49.
[27] Lamers EAD, Wijskamp S, Akkerman R. Modelling the thermo-elastic properties of skewed woven fabric reinforced composites. In: ECCM 9, Brighton, UK; 2000.
[28] Launay J, Hivet G, Duong AV, Boisse P. Experimental analysis of the influence of tensions on in plane shear behaviour of woven composite reinforcements. Compos Sci Technol 2008;68:506–15.
[29] Li X, Sherwood James, Liu Lu, Chen Julie. A material model for woven commingled glass–polypropylene composite fabrics using a hybrid finite element approach. Int J Mater Prod Tech 2004;21:59–70.
[30] Li X, Sherwood J, Liu L, Chen J. Hybrid finite element model of woven-fabric composite. In: Proceedings of the 19th annual American Society for Composites, vol. CD; 2004. p. TC-2.
[31] Li X, Sherwood J, Gorczyca J, Chen J, Liu L. A study of the thermostamping process for a woven-fabric composite. In: Third M.I.T. conference on computational fluid and solid mechanics; 2005. p. 229.
[32] Lin H, Long AC, Clifford MJ, Harrison P, van de Haar K, Akkerman R. Investigation of tool-ply friction of viscous textile composites (CD-rom). In: Long A, editor. 8th International conference on textile composites, University of Nottingham, Nottingham, UK, TEXCOMP-8; 2006.
[33] Liu L, Chen Julie, Sherwood James. Analytical model of shear of 4-harness satin weave fabrics. In: Proceedings of the 8th NUMIFORM conference paper, vol. CP712; 2004. p. 338.
[34] Liu L, Chen Julie, Sherwood James. Parametric study of commingled glass/polypropylene woven fabrics during shear. In: Proceedings of the 19th annual American Society for Composites conference, vol. CD; 2004. p. MM-6.
[35] Liu L, Chen Julie, Gorczyca Jennifer, Sherwood James. Modeling of friction and shear in thermo-stamping process—Part II. J Comp Mater 2004;38:1931–47.
[36] Liu L, Chen J. A solid mechanics shear model of commingled glass/polypropylene woven fabrics. In: Third M.I.T. conference on computational fluid and solid mechanics; 2005. p. 237.
[37] Liu L, Chen Julie, Li Xiang, Sherwood James. Two-dimensional macro-mechanics shear models of woven fabrics. Composites Part A 2005;36:105–14.
[38] Long AC, Robitaille F, Souter BJ. Mechanical modeling of in-plane shear and draping for woven and non-crimp reinforcements. J Thermoplast Compos Mater 2001;14:316–26.
[39] Lomov SV, Willems A, Verpoest I, Zhu Y, Barburski M, Stoilova T. Picture frame of woven fabrics with a full-field strain registration. Textile Res J 2006;76(3):243–52.
[40] Lomov SV, Verpoest I. Model of shear of woven fabric and parametric description of shear resistance of glass woven reinforcements. Compos Sci Technol 2006;66:919–33.
[41] Lomov SV, Barburski M, Stoilova T, Verpoest I, Akkerman R, Loendersloot R, et al. Carbon composites based on multiaxial multiply stitched preforms. Part 3: Biaxial tension, picture frame and compression tests of the preforms. Composites Part A 2005;36:1188–206.
[42] Lussier D, Chen J. Material characterization of woven fabrics for thermoforming of composites. J Thermoplast Compos Mater 2002;15(6):497–509.
[43] Lussier Darin. Shear characterization of textile composite formability. Master's thesis, Department of Mechanical Engineering at the University of Massachusetts, Lowell; 2000.
[44] Peng XQ, Cao J, Chen J, Xue P, Lussier DS, Liu L. Experimental and numerical analysis on normalization of picture frame tests for composite materials. Compos Sci Technol 2004;64:11–21.
[45] Peng XQ, Cao J. A continuum mechanics based non-orthogonal constitutive model for woven composites. Compos Part A: Appl Sci Manuf 2005;36(6):859–74.
[46] Peng XQ, Cao J. A dual homogenization and finite element approach for material characterization of textile composites. Composites Part B 2002;33(1):45–56.
[47] Potter K. Bias extension measurements on cross-plied unidirectional prepreg. Compos Part A: Appl Sci Manuf 2002;33:63–73.
[48] Wijskamp S, Lamers EAD, Akkerman R. Effects out-of-plane properties on distortions of composite panels. In: Proceedings of fibre reinforced composites 2000, New Castle, UK; 2000. p. 361–8.
[49] Xue P, Cao J, Chen J. Integrated micro/macro mechanical model of woven fabric composites under large deformation. Compos Struct 2005;70:69–80.
[50] Xue P, Peng XQ, Cao J. A non-orthogonal constitutive model for characterizing woven composite. Composites Part A 2003;34(2):183–93.
[51] Yu WR, Chung K, Kang TJ, Zampaloni MA, Pourboghrat F, Liu L, et al. Sheet forming analysis of woven FRT composites using the picture-frame shear test and the nonorthogonal constitutive equation. Int J Mater Prod Technol 2004;21:71–88.
[52] Zhu B, Teng J, Yu TX, Tao XM. Theoretical modelling of large shear deformation and wrinkling of plain woven composite. J Compos Mater [in press].
[53] Zhu B, Yu TX, Tao XM. Research on the constitutive relation and formability of woven textile composites. Adv Mech 2004;34(3):327–40.
[54] Zhu B, Yu TX, Tao XM. An experimental study of in-plane large shear deformation of woven fabric composite. Compos Sci Technol 2007;67:252–61.
[55] Zhu B, Yu TX, Tao XM. Large deformation and failure mechanism of plain woven composite in bias extension test. Key Eng Mater 2007;334–335:253–6.
[56] Zhu B, Yu TX, Tao XM. Large shear deformation of E-glass/polypropylene woven fabric composite at elevated temperatures. J Reinf Plast Compos [in press].
[57] Zhu B, Yu TX, Tao XM. Large deformation and slippage mechanism of plain woven composite in bias extension. Compos Part A: Appl Sci Manuf 2007;38:1821–8.
[58] Nestor TA, Obradaigh CM. Experimental investigation of the intraply shear mechanism in thermoplastic composites sheet forming. Adv Eng Mater 1995;99(1):19–35.
[59] Mohammed U, Lekakou C, Dong L, Bader MG. Shear deformation and micromechanics of woven fabrics. Compos Part A: Appl Sci Manuf 2000;31:299–308.
[60] Nguyen M, Herszberg I, Paton R. The shear properties of woven carbon fabric. Compos Struct 1999;47:767–79.
[61] Lebrun G, Bureau MN, Denault J. Evaluation of bias-extension and picture-frame test methods for the measurement of intraply shear properties of PP/glass commingled fabrics. Compos Struct 2003;61:341–52.
[62] http://www.techlab.fr/strain/htm#icasoft.
[63] Touchal S, Morestin F, Brunet M. Various experimental applications of digital image correlation method. In: Proceedings of CMEM 97, Rhodes (Computational methods and experimental measurements VIII); 1997. p. 45–58.
[64] De Luycker E, Boisse P, Morestin F. In: SNECMA Maia meeting, Villaroche; 2006.